SAND2019-1813C

Evaluating the Influence of Size Effects on Load-Displacement Behavior and Failure in Threaded Fasteners, Part I: Experimental Testing

Thomas R. Bosiljevac, Yuriy B. Veytskin[1], John P. Mersch[2], Jeffrey A. Smith[2], Peter W. Grimmer [2]

R&D S&E Mechanical Engineering, Experimental Environment Simulation,
Sandia National Laboratories, Albuquerque, NM, 87185

[1] Senior Scientist, Advanced Characterization & Processing Group, Savannah River National Laboratory, Aiken, SC, 29808

[2] R&D S&E Mechanical Engineering, Component Science & Mechanics,
Sandia National Laboratories, Albuquerque, NM, 87185

ABSTRACT

In an effort to enhance both the experimental testing and computational modeling of small threaded fasteners, a collaborative investigation consisting of experimental tensile testing and computational modeling was conducted to observe the effects of threaded fastener size on load-displacement behavior and failure. Experimental tests were performed on NAS1351N00-4, NAS1352N02-6, NAS1352N04-8, NAS1352N06-10, and NAS1352N4-24 (referred to herein as #00, #02, #04, #06 and #4, respectively) A286 fasteners. Displacement measurements were obtained from three unique sources/locations: Differential Variable Reluctance Transducers (DVRTs) inserted in the top bushing to measure the relative displacement of the bushing faces, Linear Variable Differential Transducers (LVDTs) located on the outside edge of the bushing fixtures to measure a more global response of the bushing displacement, and the stroke of the test frame. These tests clarified many ambiguities in the experimental process, proved the feasibility of a new test procedure and setup for small fastener testing, and added confidence in the computational models.

Keywords: threaded fastener, tensile test, fixture, bushing, DVRT

INTRODUCTION

The engineering analysis community has become increasingly interested in the simulation of threaded fastener dependent structures and is relying on the integrity of simulations as a key component of the engineering design and qualification process. However, these structures are often complex and complicated at the component level, resulting in infeasible and unrealistic material testing techniques to develop constitutive models. Since threaded fasteners are common components making up jointed connections of various geometrical shapes, sizes, and applications, this paper presents a renewed focus on experimental testing of threaded fastener size effects related to load-displacement behavior and failure. From this endeavor, advanced experimental testing methods related to fixturing and relative displacement measurements of the threaded fasteners have been implemented to clarify the many ambiguities in the experimental process and add confidence to the existing computational models.

Prior experimental tensile testing of threaded fasteners has relied on using two sources of displacement measurements. The first source was the stroke associated with the test frame actuator and the second consisted of mounting LVDTs to the fixture. The compliance in the load frame in conjunction with the location of the LVDTs led to computational models with a low-confidence analysis of simulated threaded fastener behavior and response. In addition, the NASM1312-2 fixture may introduce uncertainties to the material testing characteristics of small threaded fasteners due to the suspended weight applied to the fastener by the fixture during initial test setup and how this resulting setup-based preload might influence the stress-strain response. By improving both the proximity of the displacement sensors to the threaded fasteners and reducing the fixture weight effects during test setup, the level of confidence pertaining to the characteristic stress-strain response used by the computational modeling group can lead to a refined high-fidelity finite element model to better simulate the behavior of small threaded fasteners.

FIXTURING

The new test fixture and bushing design focused on allowing a lighter test fixture to be used while minimizing compliance issues in the load train. Additionally, the new fixture design would allow localized displacement measurements to be obtained closer to the region around the threaded fastener for the first time. The concept was to allow quasistatic tensile tests to be performed on small threaded fasteners ranging in size from #00 to #4. The specific bushings fabricated for use in the threaded fastener test series were designed for A286 stainless steel fasteners #00, #02, #04, #06 and #4, respectively. Refer to the NAS1351 and NAS1352 datasheets [1], [2]. The A286 threaded fasteners are shown below in Figure 1. The new fixturing utilized a redesigned test fixture and bushing combination made of 4340 steel heat treated to 42-46 Rockwell hardness (Rc) as referenced from the NASM1312-2 datasheet [3].

Figure 1: A286 Threaded Fasteners

The fixture assembly consists of two bushing holders and two ram adapters. The two bushing holders are identical and were fabricated with a 19 mm diameter pin hole for connecting to the ram adapters and two 12.5 mm diameter pass-through holes for routing the DVRT sensor cables to their respective data connections. The bushing holders were fabricated from 76 mm round stock in 101.6 mm lengths. The 76 mm diameter 4340 steel stock was milled with a 57 mm diameter by 62.7 mm long insertion port that then stepped down to a 38 mm diameter by 38.9 mm long bushing support sleeve. Each bushing holder weighed approximately 27 kg. The ram adapters were fabricated from 57 mm diameter by 101.6 mm long 4340 steel stock. The ram adapter consisted of a head side with a 19 mm diameter hole located in the side of the head for connecting the ram adapter to the bushing holder and a 25.4 mm-14 by 44.5 mm long female threaded connection in the end for attaching to either the actuator or upper crosshead assembly. A section view of the fixture assembly with bushings is shown in Figure 2. The fixture assembly shown in Figure 2 was rotated 180 degrees from the configuration utilized for the experimental testing.

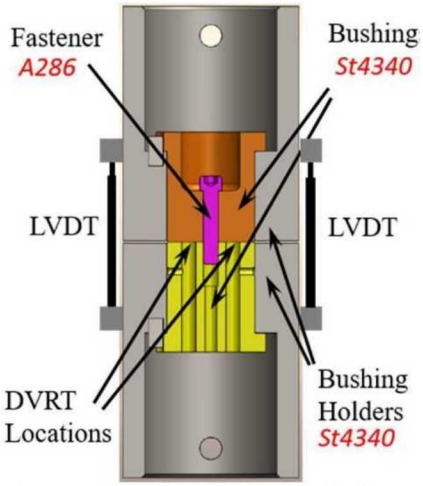

Figure 2: Section view of tensile fixture and modified bushings [4]

The bushing set for each threaded fastener size consists of two different pieces as shown in Figure 2. One piece was fabricated with threads to match the fastener size and is referred to as the threaded bushing, while the other piece was fabricated to provide an edge seat for the cap head side of the fastener and is referred to as the cap head bushing. Each bushing set shares the following common geometric design dimensions as shown in Figure 3. The overall length is 47.6 mm long with a 47.6 mm diameter by 8.3 mm thick stepped edge to properly seat into the bushing holder. Below the seat edge, the bushing maintains a 38 mm diameter over a length of 39.4 mm. The cap head bushing is shown below in Figure 3 and was modified from the standard bushing design referenced in NASM1312-2 to allow for the inclusion of four DVRT displacement sensors located 90 degrees apart and 9.5 mm from the center of the fastener as shown in Figure 3. Placing the DVRTs any closer than 9.5 mm from the center may result in fracturing during the heat treatment process.

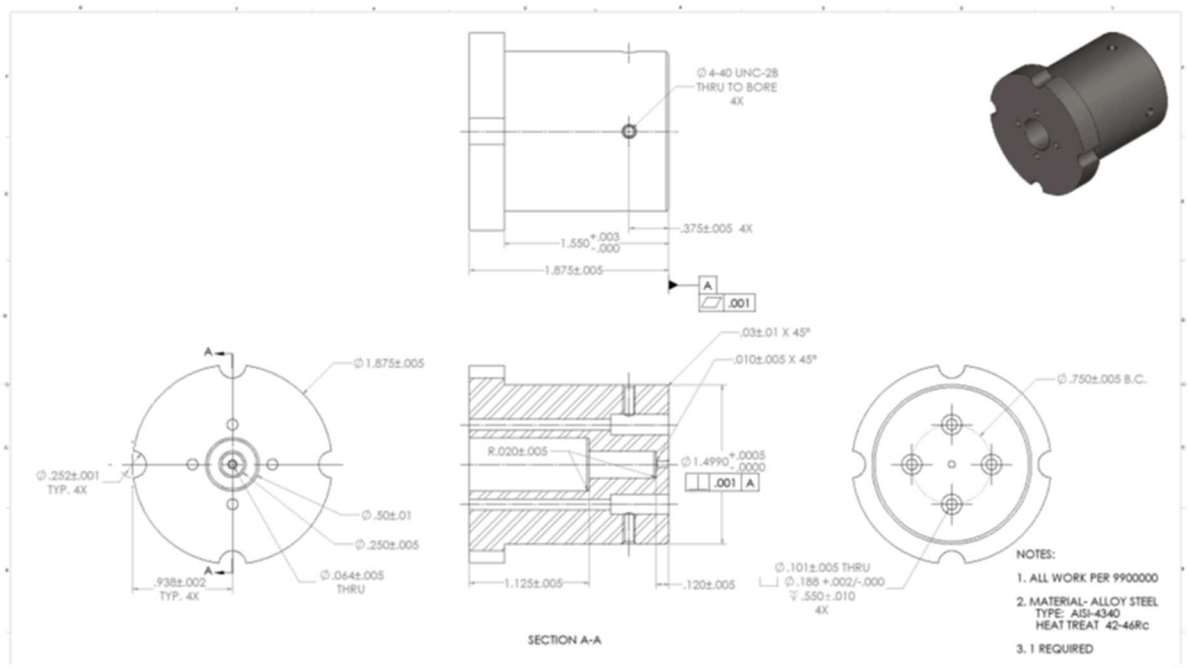

Figure 3: Cap head bushing design

DISPLACEMENT SENSORS

The DVRT displacement transducers, shown in Figure 4(a), are LORD MicoStrain, MG-DVRTs with a 1.5 mm stroke and 1.5 μm resolution. Each DVRT was inserted into an aluminum sleeve prior to positioning the sensor into the bushing, as shown in Figure 4(a). A set screw located in the side of the bushing at each DVRT location was then tightened against the sleeve to secure each DVRT into position. The DVRTs were calibrated using a Boeckler micrometer head mounted to an MTS calibration stand with a specially fabricated bushing jig to allow the time of use calibration to be performed on each individual DVRT while inserted into the bushing. Each DVRT was calibrated at increments of 0.05 mm ranging from -0.80 mm to +0.80 mm over a voltage of 0 to 5 VDC with the voltage data recorded for each calibration increment for a total of 33 data points and counted as one calibration run. The first calibration run started with the DVRTs compressed to -0.80 mm. The second calibration run was executed at the top end of the range (0.80 mm) with the third and final calibration run mimicking the first calibration run. The DVRT calibration setup is shown below in Figure 4(b). After each completed calibration, a plot of the offset versus average voltage of the three runs was used to generate a polynomial fit using the trendline feature in Excel. Each sensor's polynomial expression was then loaded into the sensor setup file to allow for data acquisition based on the input voltages recorded during testing. After calibration, each sensor number was labeled on the bushing to ensure alignment of the four DVRTs with the four LVDTs.

(a) (b)

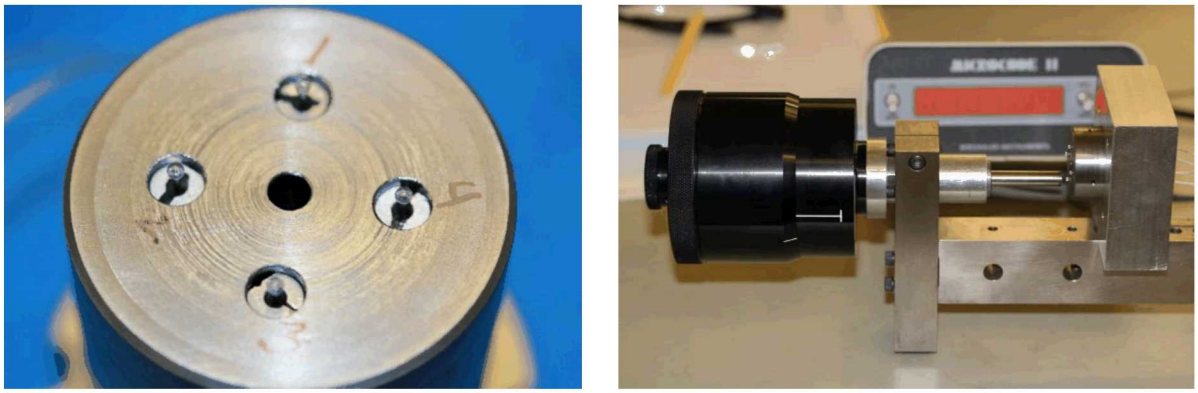

Figure 4: (a) Position of DVRTs in bushing; (b) DVRT calibration setup

A time of use calibration was also performed on each LVDT. The calibration was conducted using the Boeckler micrometer head mounted to the calibration stand. The LVDTs used were Macro Sensor BBP315 sensors with a 5 mm range. Each LVDT was calibrated from -2.5 mm to +2.5 mm at a coarse increment of 0.254 mm from +/-2.54 mm to +/-0.381 mm before switching to a 0.0508 mm increment between -0.381 and 0.381 mm for a total of 33 data points.

QUASISTATIC TENSILE TEST SETUP

A 100 kN MTS load frame was selected based on the load range of the small threaded fasteners. To ensure fidelity with the load data, a 45 kN load cell was added below the load frame's 100 kN load cell. An annual calibration was performed on the 100 kN load frame's 100 kN load cell and 15cm stroke actuator. In addition, an annual calibration was completed on the auxiliary 45 kN load cell. The load cells and actuator were calibrated to a tolerance of 1% of applied force or displacement. An MTS Flextest 60 modular controller was used for transducer conditioning and data acquisition. The output signals captured were the load cell, auxiliary load cell, stroke, LVDTs and DVRTs. The MTS MultiPurpose TestWare (MPT) was used to write the tensile test procedure for each test. The rate of pull input into the test procedure was load-controlled. A break detect command would then trigger a stop to the tensile test and place the frame back into stroke control.

The complete tensile test setup, shown in Figure 6, consisted of an upper and lower fixture assembly. The upper bushing assembly was supported by the frame's crosshead and consisted of a 100 kN load cell threaded together with a 45 kN auxiliary load cell, which was then connected to the upper ram adapter. The lower bushing assembly consisted of the lower ram adapter threaded to the frame's actuator. The threaded fastener was first inserted into the cap head bushing containing the four DVRTs which was then inserted into the upper bushing holder and adjusted such that each DVRT number label matched the corresponding LVDT number label, located on the outside of the upper bushing holder. The four DVRT sensor cables were routed through the two 12.5 mm pass-through ports located in the bushing holder. The cap head bushing holder was placed in a horizontal positioner, and the lower bushing holder containing the threaded bushing was aligned with the upper bushing holder to allow the threaded fastener to be threaded into the lower bushing, which coupled the upper and lower bushing holders together. The upper bushing holder was then connected to the upper ram adapter via a 19 mm diameter pin before manually controlling the actuator to align the lower ram adapter with the lower bushing holder and install the 19 mm diameter pin.

(a) (b)

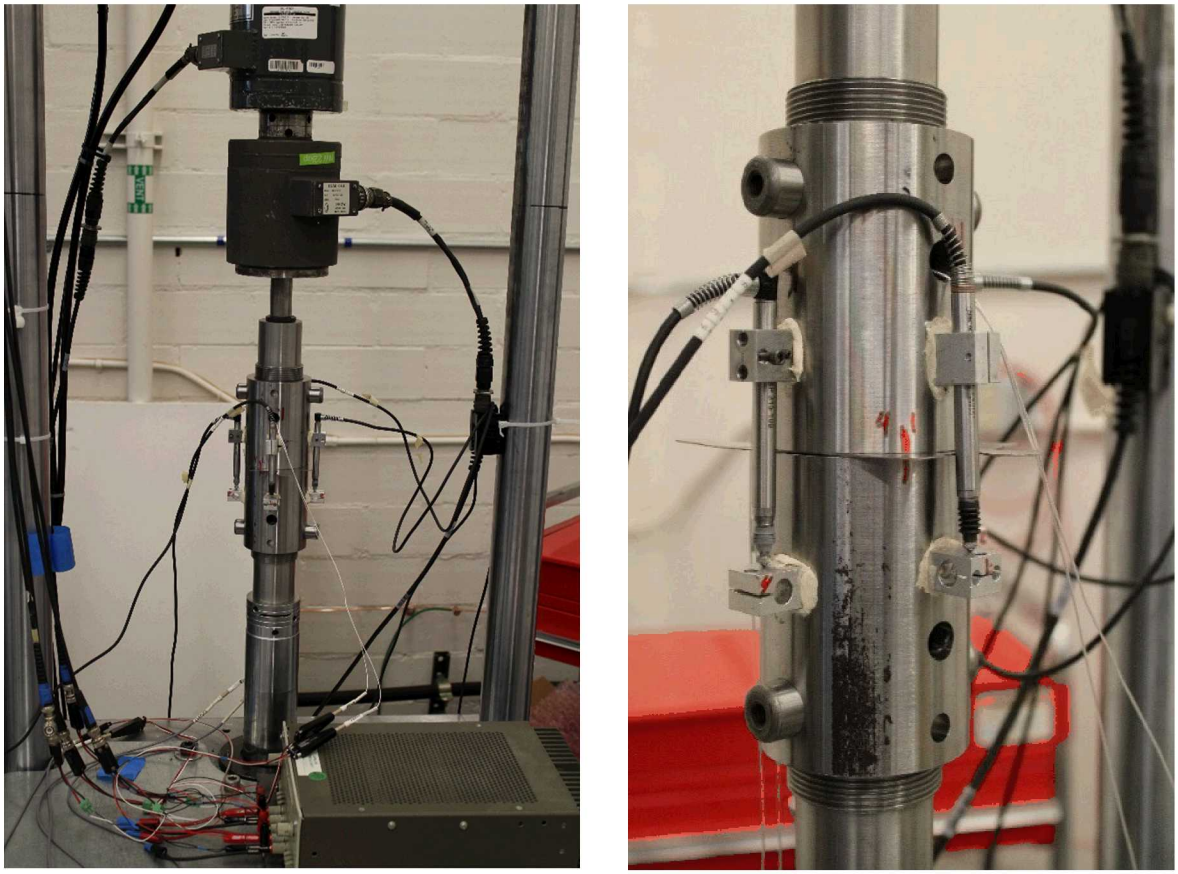

Figure 6: (a) Tensile test setup in 100 kN load frame; (b) Close-up view of test setup

QUASISTATIC TENSILE TESTING

The sequence of threaded fastener testing began with the #00 threaded fastener size and progressed up through each size before concluding the test series with the #4 size. A minimum of three successful tests was required prior to moving on to the next size in the test series. The stroke rate applied to each of the threaded fasteners was based a strain rate of 0.0005 times the gage length of the fastener. The gage length was taken as thickness of the bushing supporting the hex head side of the fastener. Using these known gage lengths, the applied test rate for each size fastener was calculated as 0.0015 mm/s for the #00, 0.0022 mm/s for the #02, 0.0028 mm/s for the #04, 0.0036 mm/s for the #06, and 0.029 mm/s for the #4.

Before each series of threaded fastener tests began, several linearity checks were run to determine the behavioral relationship between stroke, LVDTs, and DVRTs. Ideally, the relationship would be as close as possible to a 1:1 with the stroke. The linearity check was performed using two methodologies. The first was with no threaded fastener placed in the upper bushing and the second included a threaded fastener in the upper bushing. Regardless of which linearity methodology is utilized, the upper bushing holder containing the bushing would be attached to the upper ram adapter and the lower bushing holder containing the threaded side bushing would be completely lowered until the threaded side bushing makes contact with the lower ram adapter, as shown in Figure 7. The actuator was then raised until the two bushings came into contact and the DVRTs were compressed to an electrical voltage signal of 4.6 Volts, which corresponded to a compressed displacement of approximately 1.45 mm.

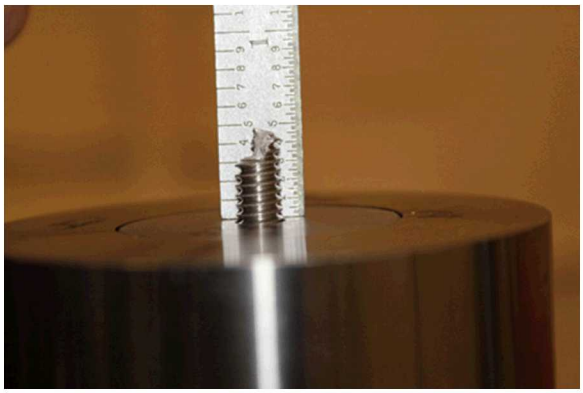

Figure 7: Thread side bushing in bushing holder

The linearity check utilized the same applied rate as required for the fastener size being tested. The linearity check concluded when approximately 0.5 to 1 mm of displacement had occurred. The output data from each DVRT and LVDT versus stroke was then plotted to check the linearity of the measurement devices. Examples of these linearity check (sensor check) plots are shown below in Figure 9. The DVRTs showed more variation, while the LVDTs tended to remain within 2% with the stroke. DVRT1, DVRT2 and DVRT4 showed the least amount of variation, which tended to range from 1.5 to 17%. DVRT3 consistently showed the most variation (1%3 to 30%) compared to the other DVRTs in each linearity check and, as a result, was removed from the data set when calculating the average strain used to plot the stress-strain curves related to DVRT displacements. It should be noted that two to three linearity checks were run for each fastener size. If a linearity check resulted in an average variation amongst DVRT1, DVRT2 and DVRT4 greater than 10%, the DVRTs were re-calibrated and the linearity checks were re-run. Upon completion of the linearity check, the particular threaded fastener test series was carried out. The output data from each of the threaded fastener test series was then reduced to produce stress-strain curves.

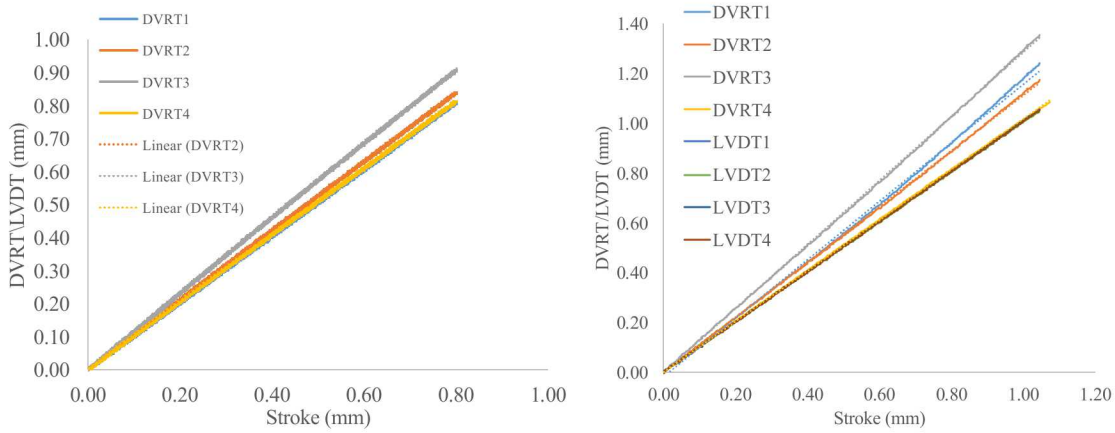

Figure 9: (a) #06 linearity plot DVRT vs Stroke; (b) #4 linearity plot DVRT/LVDT vs Stroke

RESULTS

The quasistatic tensile test stress-strain curves for each threaded fastener size tested are shown below in Figure 10. Each of the stress-strain curves includes strain calculated based on the DVRTs and the LVDTs. DVRT-related strains were obtained by taking the average strains from only three of the four sensors (DVRT1, DVRT2 and DVRT4, respectively). The LVDT-related strains were based on taking an average from all four sensors. The DVRT stress-strain curves for each threaded fastener size are shown as a solid line, while the LVDT stress-strain curves are shown with dashed lines. The stress-strain curves provide clear insight related to the size relationship on load-displacement behavior and failure in the threaded fasteners. The smaller #00 and #02 threaded fasteners have slightly lower peak stresses (1,300 MPa) when compared to the larger threaded fasteners (1,500 MPa), but the strain at which peak and failure stresses occur is significantly different. The #00 and #02 threaded fasteners show a strain at failure of almost 0.17 mm/mm, while the #04 and #06 threaded fasteners have strains at failure of approximately 0.07-0.08 mm/mm, with the #4 threaded fasteners failing at a strain of approximately 0.05 mm/mm based on the DVRT related strain [4]. This trend of decreasing strain at failure with increasing fastener size is

as expected given that the lower fastener sizes are more ductile with higher plasticity, based on their annealed microstructures which will be discussed in the Failure Analysis section. The trend of increasing ultimate tensile strength (peak stress) for increased fastener size is also as expected since the larger fastener sizes are cold worked, which increases ultimate tensile strength at the expense of greater brittleness. Energy absorption is an important quantity in failure prediction, so a measure of the energy density dissipated by each fastener is computed by calculating the area under the curves (using Simpson's Rule[5]) in Fig. 6. The #00 and #02 fasteners that exhibit lower yield and higher ductility have failure energies of 23.1 lbf-in/in3 and 23.4 lbf-in/in3, respectively, while the #04, #06, and #4 fasteners that have higher yield stress and lower ductility have failure energies of 12.9 lbf-in/in3, 10.8 lbf-in/in3, and 12.5 lbf-in/in3, respectively, approximately a 50% reduction in energy absorption.

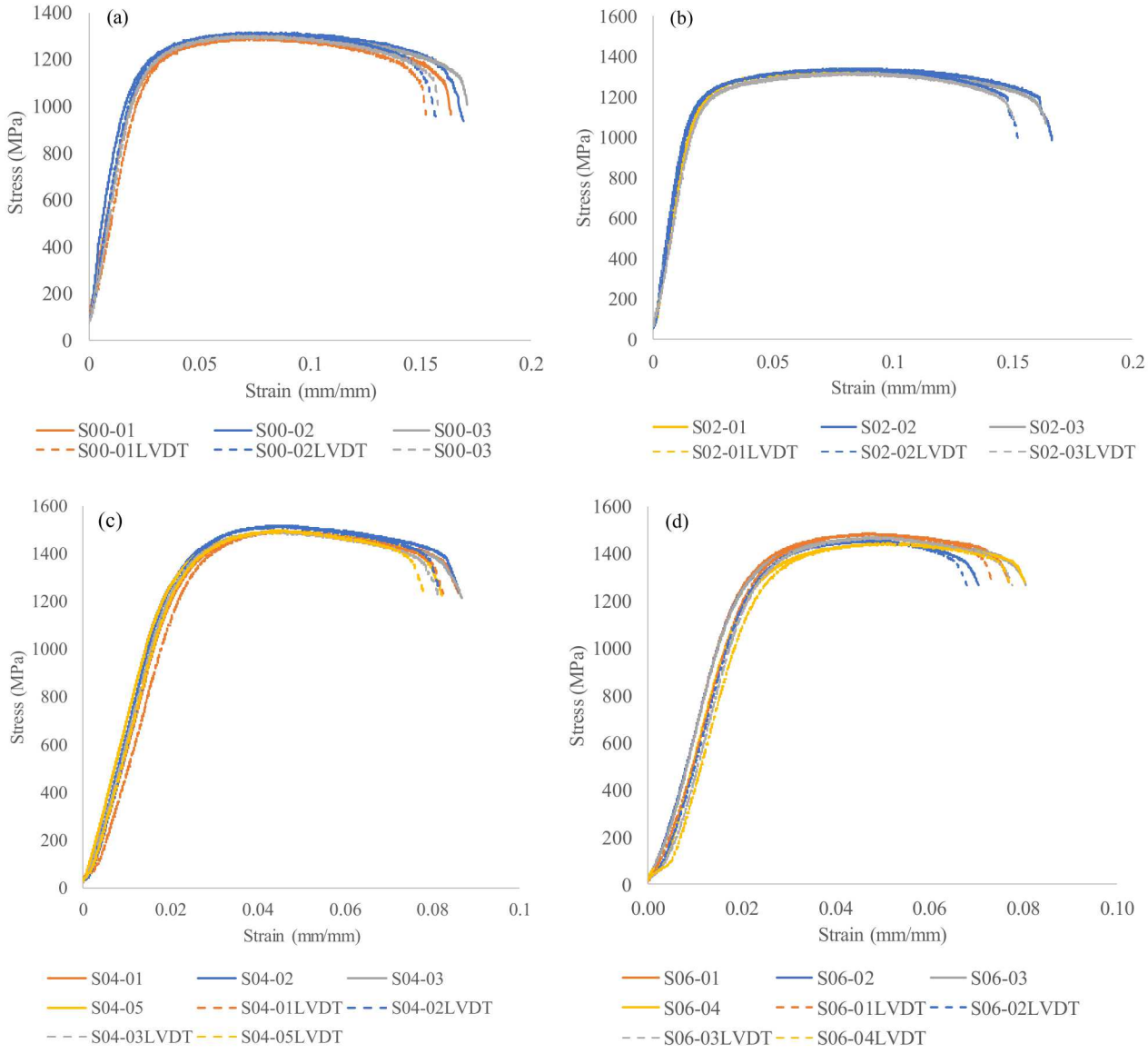

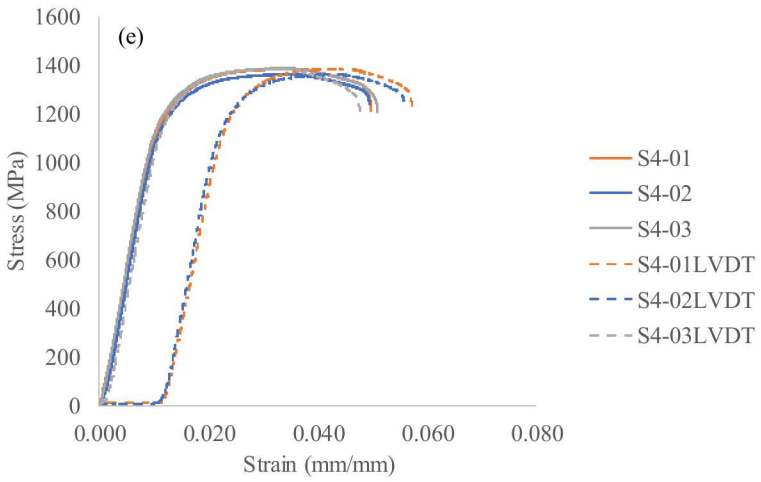

Fig. 10: LVDT and DVRT stress-strain curves for (a) #00; (b) #02; (c) #04; (d) #06; (e) #4

One other noticeable effect relates to the difference in LVDT and DVRT strain at failure. In almost all the fasteners tests, a difference of 0.01 mm/mm is seen between the LVDTs and DVRTs strains. Other observational results are shown in the figures below of tested threaded fastener specimens. Figure 11 shows a #04 fastener failure of the specimen still threaded into the lower bushing with the cap head half standing up behind for comparison. Figure 12 shows the typical modes of failure, with the most common type of fracture being a step fracture occurring over two threads. The largest size, #4, in Figure 12(b) shows a 90° failure of the bulk bolt, suggesting brittle failure which occurs at a normal plane of 90° from the loading axis. The smaller sizes suggest closer to a 45° fracture to the loading axis, as expected for more ductile materials. However, note that because of the helical geometry of the threads, traditional interpretations of specific angles associated with ductile or brittle fracture have less clarity in these complex geometries. Additionally, the #4 fastener has a larger non-threaded region than the other sizes, further complicating direct comparisons.

Figure 11: #04 threaded fastener failure

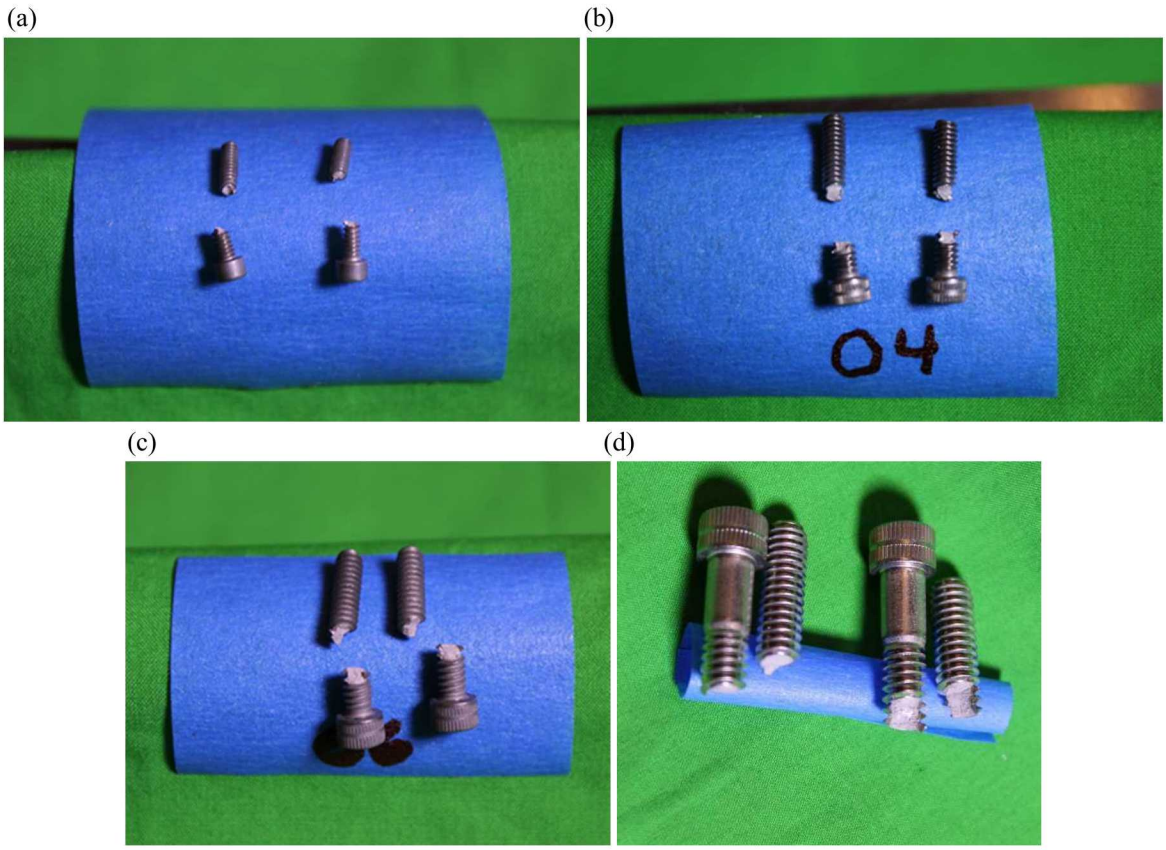

Figure 12: (a) #00 failure specimen; (b) #04 failure specimen; (c) #06 failure specimen; (d) #4 failure specimen

ANALYSIS

A failure analysis can be conducted based on electron backscatter diffraction (EBSD) images collected of the same fractured specimens for microstructure-property relationships. The stark differences between the strength and ductility of the #00 and #02 fasteners and the #04, #06, and #4 fasteners motivated a microstructural investigation. EBSD maps, captured from a scanning electron microscope, of an untested #02 and #06 fastener are shown in Figures 13 and 14, respectively. Note Figures 13 and 14 show the Inverse Pole Figures with respect to the "x direction" (IPF X), which is along the axis of the fastener. The #02 fastener map is morphologically (structurally) representative of the #00 and #02 group, and the #06 fastener map is morphologically representative of the #04 and #06. No EBSD has been performed on the ¼" specimens. The grain structure is very different in the two fasteners, as the grains in the #06 tend to be elongated with a columnar pattern, and have evidence of cold work through the preferential axis orientation in the #06 fastener whereas the grains in the #02 fastener are equiaxed, indicating an annealed structure (as opposed to cold-worked), with more clearly defined grain boundaries in the EBSD map. Note that, while the grain structure indicates a cold- worked vs. annealed structure, all of the fasteners have been subsequently precipitation strengthened (age hardened) to a high-strength condition. In both Figures 13 and 14, the distributions of the colors of the inverse pole figures are similar, suggesting that the crystallographic grain orientations are preferred to similar extents in both fasteners, however Figure 13 shows more affinity for the <1 1 1> Euler-based axis (blue) and <001> (red) along the axis of the cold- worked fastener while <1 0 1> (green) is less prevalent, especially in the central region of the fastener. It is known that cold working deforms metal grain structures, as observed in Figure 14, and creates a "locking effect" from the entanglement of generated dislocations, which causes increased yield and ultimate tensile strengths and reduced deformation, all of which are represented in Figure 10 when comparing the #00 and #02 "annealed" fastener group to the #04 and #06 "cold worked" fastener group. It is known that annealing increases ductility by reducing the number of dislocations and increasing the number of slip conditions at grain boundaries, and this increased ductility is represented by an increased strain to failure for the #00 and #02 fastener group in Figure 10. The correlation between the microstructure and

load-displacement behavior suggests that EBSD mapping of the #4 fastener will reveal it is structurally similar to the #04 and #06 sizes.

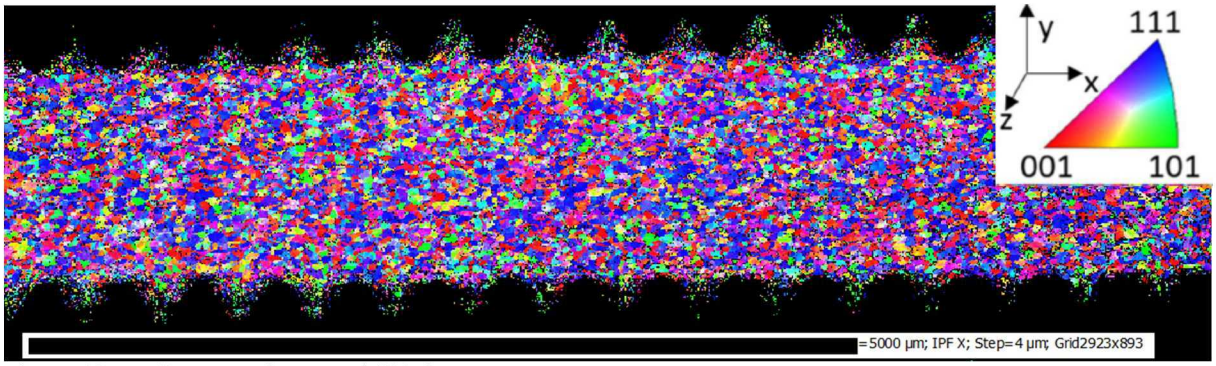

Figure 13: EBSD map of untested #02 fastener

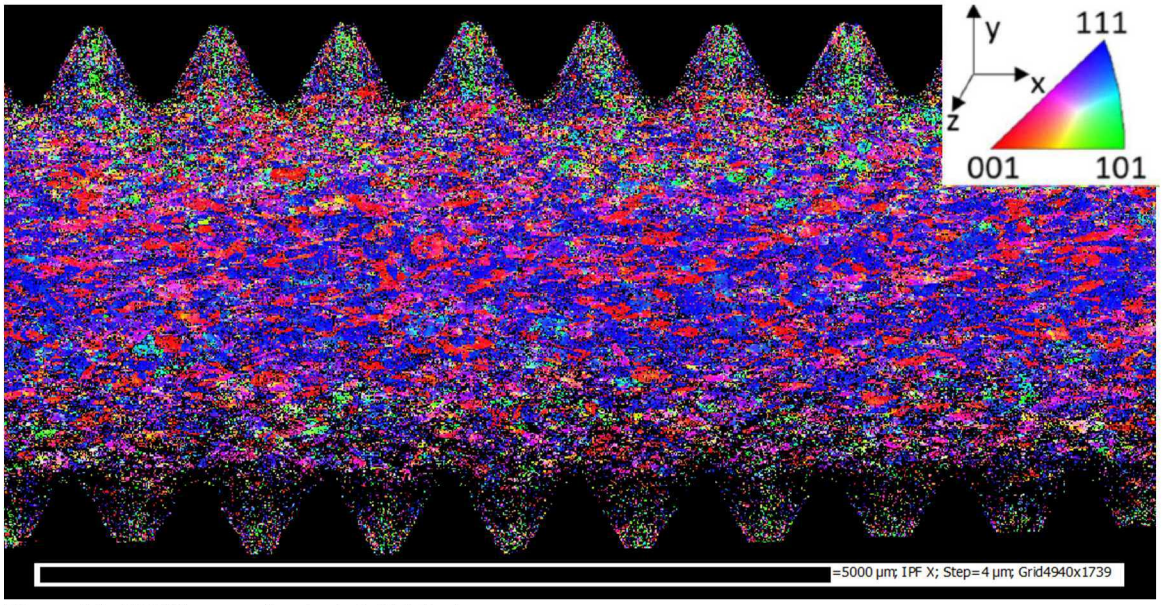

Figure 14: EBSD map of untested #06 fastener

A fractured #02 fastener is shown in Figure 15. The angle of the fracture supports a ductile failure regime, as expected, and there is also some grain deformation in the region of the fracture where a transition from equiaxed to columnar grains appear to occur for this size, in addition to a greater preference for the <1 1 1> direction.

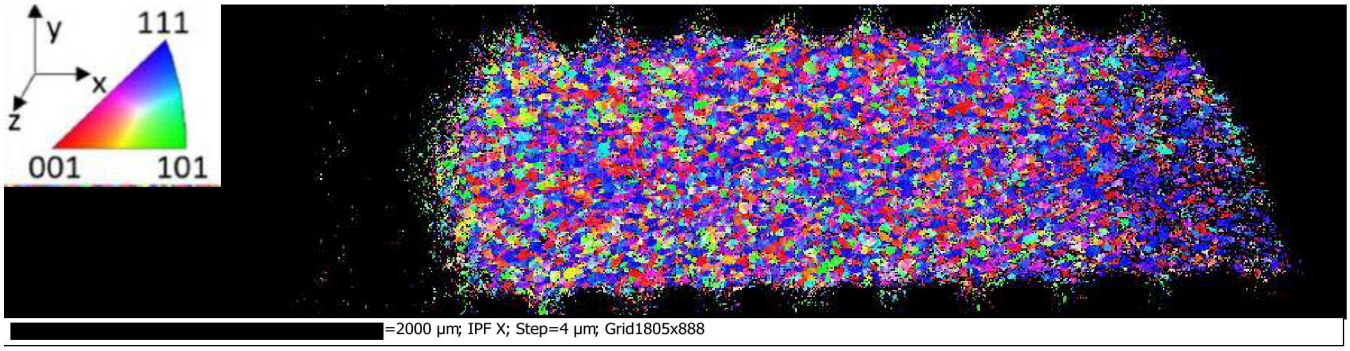

Figure 15: EBSD map of tested #02 fastener

Lastly, Figure 16 shows a tested #06 fastener. The fracture is brittle; however, an interesting observation is that because fracture always occurs between thread roots, the angle of the fracture is diverted to reach the nearest thread root. This is thus a geometric effect that overpowers other inherent effects.

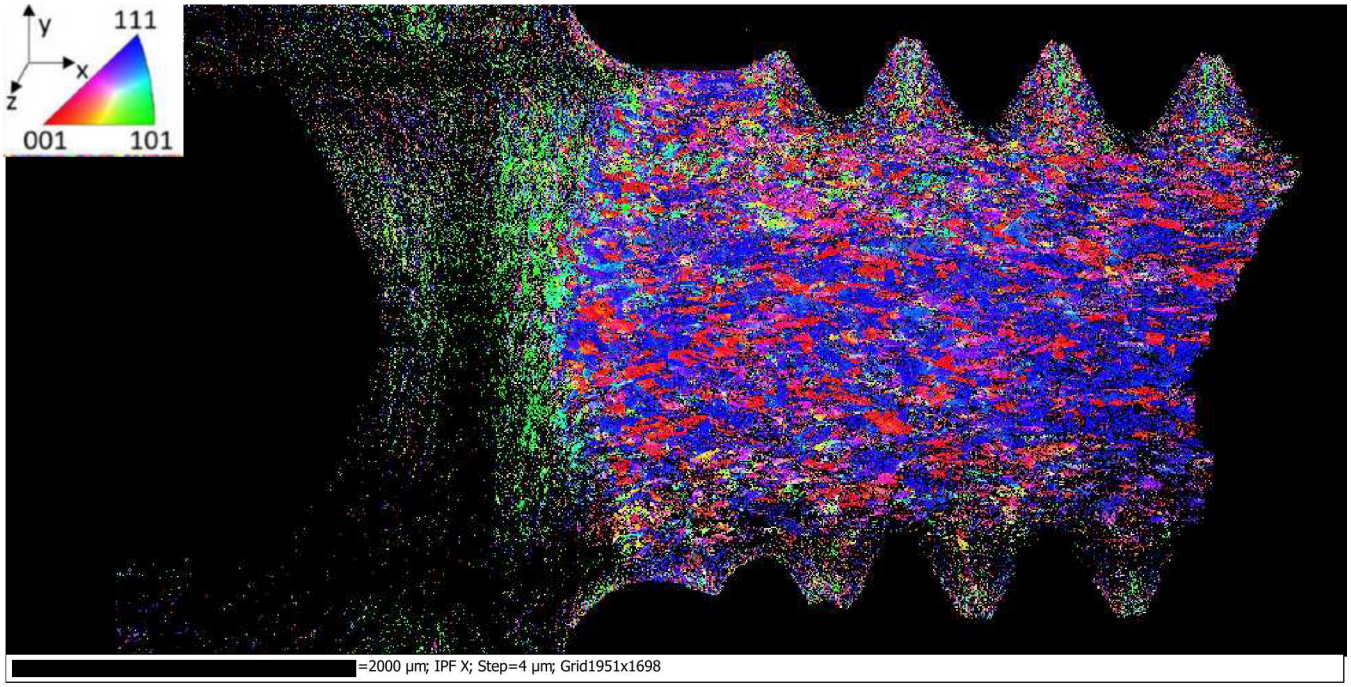

Figure 16: EBSD map of tested #06 fastener

CONCLUSION

A collaborative investigation consisting of experimental tensile testing and computational modeling was conducted to observe the effects of threaded fastener size on load-displacement behavior and failure. The quasistatic tensile testing and microstructural investigations have shown a threaded fastener size relationship pertaining to load-displacement behavior, including ultimate tensile strength, ductility, and absorbed energy. Microstructural analysis has revealed fundamental characteristics of the material and provided the necessary link for structure-property relationships.

The placement of DVRT sensors closer to the threaded fastener being tested, in conjunction with LVDTs, has added confidence in the mechanical properties and behavior of small threaded fasteners used in computational modeling.

A microstructural investigation revealed differences in the material of the #02 and #06 fasteners, which explains the differences between the engineering stress-strain response of the smaller (#00 and #02) and larger (#04, #06, and #4) fasteners. The analysis results suggest that independent calibrations do not extrapolate well to fasteners that have different microstructures. Furthermore, the analysis models did not reveal an underlying structural size effect that could guide extrapolation across sizes; rather, it appears that the differences in the load-displacement response of the different sized fasteners are mostly dominated by differences in their inherent material properties. This consequently makes it challenging to guide fastener modeling in the absence of empirical load-displacement test data. Future work should attempt to link specification and manufacturing information to the load-displacement response of a given fastener to improve blind predictions of fastener performance in the absence of direct test data on the fastener of interest.

ACKNOWLEDGEMENTS
The authors would like to thank Edmundo Corona, John Mersch, and Jeff Smitth of Sandia National Laboratories for feedback and refinement to promote a collaborative atmosphere. Sandia National Laboratories is a multimission laboratory managed and operated by National Technology and Engineering Solutions of Sandia, LLC, a wholly owned subsidiary of Honeywell International, Inc., for the U.S. Department of Energy's National Nuclear Security Administration under contract DE-NA0003525.

REFERENCES

[1] AIA/NAS – Aerospace Industries Association of America Inc., 2016, "English -- Screw, Cap, Socket Head, Undrilled and Drilled, Plain and Self-Locking, Alloy Steel, Corrosion-Resistant Steel and Heat-Resistant Steel, UNRF-3A - Rev 10", AIA/NAS NAS1351

[2] AIA/NAS – Aerospace Industries Association of America Inc., 2016, "English -- Screw, Cap, Socket Head, Undrilled and Drilled, Plain and Self-Locking, Alloy Steel, Corrosion-Resistant Steel and Heat-Resistant Steel, UNRC-3A AND UNRC-2A - Rev 13", AIA/NAS NAS1352

[3] AIA/NAS – Aerospace Industries Association of America Inc., 2012, "English – Fastener Test Methods-Method 2-Interactions", AIA/NAS NASM1312-2

[4] Grimmer, P.W., Mersch, J. P., Smith, J. A., Veytskin, Y.B., Susan, D.F., "Modeling Empirical Size Relationships on Load-Displacement Behavior and Failure in Threaded Fasteners" 2019 AIAA/ASCE/AHS/ASC Structures, Structural Dynamics, and Materials Conference, AIAA SciTech Forum, AIAA2019-2268, San Diego, CA, 2019

[5] "Integration and ODEs, Scipy.org, 05/05/2018, https://docs.scipy.org/doc/scipy/reference/integrate.html, Accessed 10/2018